Modification of Activated Carbon Fiber by Metal Dispersion and Surface Functionalization for the Removal of 2-Chloroethanol

ARTICLE *in* INDUSTRIAL & ENGINEERING CHEMISTRY RESEARCH · JANUARY 2011

Impact Factor: 2.59 · DOI: 10.1021/ie101860e

5 AUTHORS, INCLUDING:

Mekala Bikshapathi
Indian Institute of Technology Kanpur
6 PUBLICATIONS **73** CITATIONS
SEE PROFILE

Ashutosh Sharma IITK
Indian Institute of Technology Kanpur
336 PUBLICATIONS **7,421** CITATIONS
SEE PROFILE

Nishith Verma
Indian Institute of Technology Kanpur
129 PUBLICATIONS **1,303** CITATIONS
SEE PROFILE

I&EC research
Industrial & Engineering Chemistry Research

ARTICLE

pubs.acs.org/IECR

Modification of Activated Carbon Fiber by Metal Dispersion and Surface Functionalization for the Removal of 2-Chloroethanol

Mekala Bikshapathi,[†] Susovan Mandal,[‡] Gyanesh N. Mathur,[†] Ashutosh Sharma,[†,§] and Nishith Verma*[,†]

[†]Department of Chemical Engineering, [‡]Department of Chemistry, and [§]DST Unit on Nanosciences, Indian Institute of Technology Kanpur, Kanpur-208016, India

ABSTRACT: Nickel-impregnated phenolic resin precursor-based activated carbon fiber (ACF) was functionalized with pyridine and investigated for the adsorptive removal of 2-chloroethanol. Adsorption tests were carried out under flow conditions for different gas flow rates, solute concentrations, and temperatures in a perforated tubular adsorber. Various analytical and spectroscopic techniques, including X-ray diffraction (XRD), Fourier transform infrared (FT-IR) spectroscopy, scanning electron microscopy (SEM), and CHNSO elemental analysis, were used to characterize the adsorbents that have been prepared in this study. The results showed that the ACFs adsorbed significant amounts of 2-chloroethanol. Temperature had adverse effects on adsorption. At metallic concentrations in excess of 0.4 M of nickel, the formation of metal crystallites occurred, causing blockage of the pores and a decrease in the number of active metal sites. The functionalization of ACFs by pyridine was shown to produce a basic surface, resulting in the enhanced adsorption of the organic solute. The results have applications in the preparation of effective ACF-based adsorbents for controlling the emission of hazardous organic compounds.

1. INTRODUCTION

There are several harmful gaseous organic compounds emitted in the atmosphere from the automobile, petroleum, and chemical industries. Significant amounts of such pollutants are also emitted because of the combustion of gases, and during the transport, handling, storage, and usage of the liquid organic solvents. These compounds may be hazardous to the ecosystem, and human health, upon exposure, even at low concentration levels.

2-Chloroethanol ($HOCH_2CH_2Cl$) is an organochlorine compound that has characteristics of both an alcohol and a chlorinated hydrocarbon. Although it is widely used as an insecticide, and as a solvent in many chemical industries, it is toxic and mutagenic.[1,2] Its vapor is highly toxic, because, in tissue, it can hydrolyze to form hydrochloric acid, and it may be fatal, causing damage to the central nervous system, kidneys, and liver.[3,4] Similar to many organochlorine compounds, 2-chloroethanol, upon combustion, produces hydrogen chloride (HCl), and phosgene, which are also highly toxic. Traces of 2-chloroethanol can also be found in groundwater.[5]

Risk and exposure assessments, along with the development of disposal strategies for such chemicals, are necessary in case of the inadvertent release of the chemicals into the atmosphere. It is equally necessary to develop a suitable method to control the emission of these compounds, in case of any such an eventuality. Adsorption is a potential option in this context.

There are several studies on the development of granular activated carbon (GAC) and metal-impregnated GAC as adsorbents for the removal of common atmospheric gases (for example, SO_2, NO_x) and volatile organic compounds (VOCs) (such as benzene, toluene, and xylene (BTX)), as well as toxic gases (for example, phosgene, hydrogen cyanide, and arsine).[6−11] The GAC-based adsorbents have also been used for the destruction and/or disposal of toxic and hazardous chemicals.[12] The main disadvantages of GAC-based adsorbents are significant diffusional mass-transfer and hydrodynamic resistances. In addition, a maldistribution of flow may occur, because of channeling in an adsorber packed with granular particles, resulting in underutilization of the adsorbents.

In recent years, activated carbon fibers (ACFs) have attracted much attention, because of their widespread applications in environmental remediation. In particular, ACF is shown to be capable of effectively removing common atmospheric air pollutants, such as VOC, SO_2, and NO_x. In addition, ACFs that have been impregnated with transition metals (such as Ni, Cu, and Cr) have been shown to be effective in adsorbing several air and water pollutants.[13−21] The surface of ACFs can be functionalized with suitable reagents to render it acidic or basic, depending on the type of contaminants to be removed.[22−25]

ACF has advantages over its traditional counterpart, GAC, because of their larger kinetic rates, uniform pore size distribution (PSD), lesser mass-transfer and hydrodynamic resistances, larger thermal conductivity, lower density, flexibility, and ease of handling. This makes ACFs suitable in several special applications. As an example, an ACF cloth can be wrapped over the perforated section of a tubular adsorber. The pressure drop in such an arrangement is also found to be smaller than that in the traditional adsorbers packed with granular particles.[7] ACF can be surface-functionalized with suitable reagents, depending on the type of the solute (acid or basic, hydrophobic or hydrophilic) to be controlled. In these contexts, ACFs seem to be a potential candidate to be developed and tested as an adsorbent for

Special Issue: Ananth Issue

Received: September 5, 2010
Accepted: November 11, 2010
Revised: November 6, 2010
Published: January 14, 2011

the removal of 2-chloroethanol, which is a hazardous organic compound.

In this study, the main objective is to prepare ACFs that have been impregnated with nickel and functionalized by pyridine, a basic reagent, for the adsorption of 2-chloroethanol and to test its adsorptive characteristics. The incorporation of nickel was carried out by the incipient wetness impregnation method under flow conditions, followed by calcinations and reduction. Surface functionalization was carried out by the reflux of pyridine vapors. Adsorption tests were carried out under flow conditions for different gas flow rates, solute concentrations, and temperatures. A perforated tubular adsorber wrapped with ACF cloth was used for the tests. Nickel loading and the surface basic functional groups were determined to influence the performance of the prepared adsorbents.

2. EXPERIMENTS

2.1. Preparation of Nickel-Impregnated ACFs. Reagent-grade 2-chloroethanol, nickel nitrate ($Ni(NO_3)_2 \cdot 6H_2O$), and pyridine (>99%) were obtained from Merck (Germany). Nitrogen (>99%), hydrogen (>99%), and zero air (>99%) were obtained from Sigma Gases. Analytical reagent (AR)-grade acetone was obtained from SD Fine Chemicals (Mumbai, India). The phenolic resin-based ACF was supplied by Nippon Kynol, Inc. (Japan).

The as-received samples of fibers were leached by dipping them in deionized (DI) water for ~6 h at 80 °C, to remove any undesirable ions from the surface and to render the subsequent steps (impregnation, etc.) effective. The ion analysis of the spent water showed chlorides, nitrates, and phosphate ions in the range of 1−5 ppm. The washed ACF was dried at 110 °C in an oven for 12 h. Nickel impregnation was carried out using the incipient wet-impregnation technique for 6 h under flow conditions, using a peristaltic pump. Acetone solution was used as a solvent for nickel(II) nitrate hexahydrate ($Ni(NO_3)_2 \cdot 6H_2O$) crystals. The solubility of nickel salt in acetone was experimentally measured as ~133 g/100 mL at 25 °C. This compares to 238.5 g/100 mL in water at 20 °C.[26] ACF was wrapped over the perforated tube. The details of the experimental setup and arrangement for impregnation may be obtained from our previous study on the removal of arsenic using iron-impregnated carbon fibers.[18]

The solutions of different concentrations (0.1−1.0 M) of nickel in acetone were prepared to obtain varying nickel loadings on ACF. In a recent study, we have shown that impregnation using organic solvent is more effective than water in transferring metal ions from the bulk solution to the surface of the ACF, because of its hydrophobicity toward acetone.[16] After impregnation, wet samples were dried in static air at 40 °C for 6 h, followed by drying in the oven at ~120 °C for 12 h.

The second step of the preparation was calcination. In this step, the dried nickel-impregnated ACF was subjected to heat treatment in an oven at 300 °C for 1 h to convert $Ni(NO_3)_2 \cdot 6H_2O$ to NiO:

$$Ni(NO_3)_2 \cdot 6H_2O(s) \rightarrow NiO(s) + 2NO_2(g) + \frac{3}{2}O_2(g) + 6H_2O(g)$$

The calcined material (ACF loaded with NiO) obtained in the second step was subsequently reduced by hydrogen. In this step, the calcined samples were transferred in a vertical quartz tubular reactor that was mounted in a vertically movable high-temperature furnace.

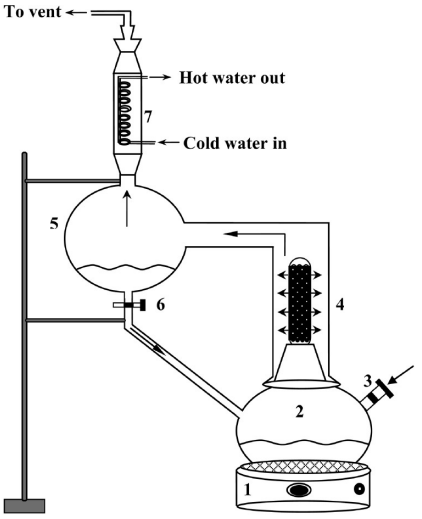

1. Heating mantle 2. Reagent flask 3. Inlet port for filling pyridine 4. ACF wrapped over perforated tube 5. Collector flask 6. Outlet to recycle condensate 7. Water condenser

Figure 1. Schematic diagram of the experimental setup for surface functionalization of ACF.

The temperature of the furnace was slowly increased, at the rate of 5 °C/min, from the room temperature to the reduction temperature (500 °C). Reduction was carried out for 1 h in hydrogen flow at 150 cm^3 per min to convert NiO to its metallic state. The details of the equipment used for calcinations and reduction are also available in our previous study.[18] After reduction, the samples were allowed to cool slowly to room temperature under a small N_2 flow rate (0.15 slpm).

2.2. Surface Functionalization. Figure 1 is a schematic of the experimental setup that was designed, fabricated, and used in this study for the surface functionalization of ACF. The setup primarily consisted of a round-bottomed (RB) glass flask that was mounted in a heating mantle. The temperature was controlled with the aid of a proportional integral derivative (PID) controller. The top (neck) of the flask was fitted with a glass tube (with an inner diameter of ID = 0.635 cm and a length of L = 8 cm). The other end of the tube was sealed (closed). The longitudinal section of the tube was circumferentially perforated with 1-mm holes at a pitch of 1 mm. The sample of ACF was wrapped over the perforated section of the tube. An arrangement was made to transfer pyridine solution into the reagent flask. Upon heating, vapors of pyridine rose from the flask into the tube and passed radially outward through the perforations and the bed of ACF to the collector flask. The vapors were condensed using the double jacketed water condenser attached to the top of the collector flask. The condensate collected in the collector flask was recycled back to the reagent flask.

For functionalization of ACF (~2 g), 100 mL of the pyridine solution was filled in the reagent flask. The strength/purity of the pyridine solution was 99.5% (w/w). The solution was heated to ~120 °C with the help of the heating mantle. Upon heating, pyridine vapors passed through the bed of ACF wrapped over the perforated tube and subsequently condensed in the condenser and collected in the collector flask. The surface functionalization was carried out for 8 h. The condensed vapors were recycled several times during functionalization. The functionalized

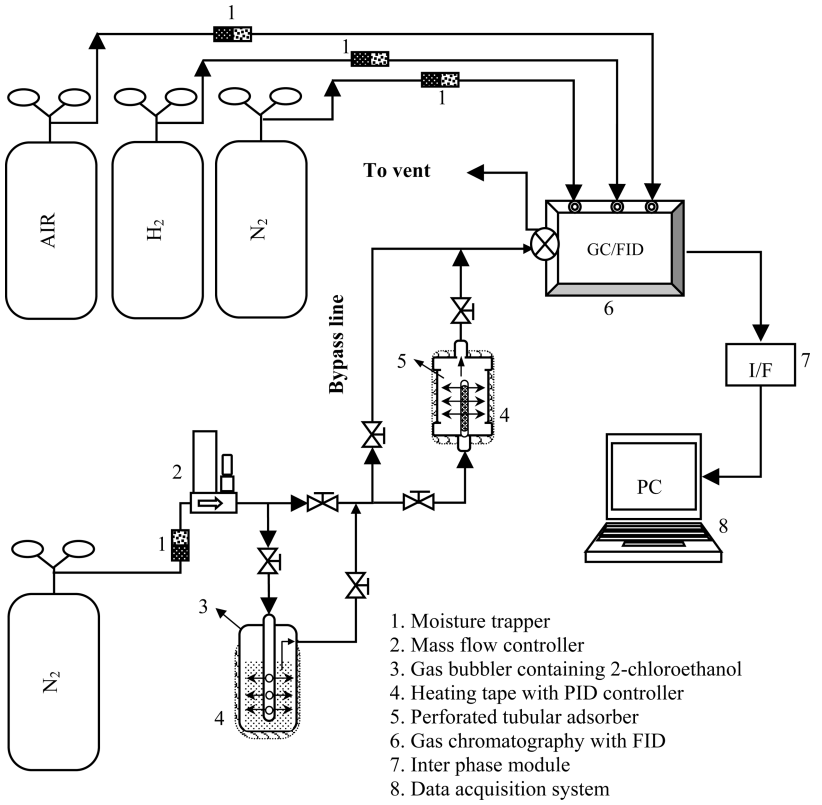

Figure 2. Schematic diagram of the experimental setup for breakthrough analysis.

ACF were then dried at 40 °C for 12 h, before using them for the subsequent characterization and adsorption tests. For adsorption, the freshly functionalized samples were prepared and used immediately.

2.3. Adsorption. Figure 2 is a schematic of the experimental setup designed and fabricated to study the adsorptive removal of 2-chloroethanol under flow conditions. The 2-chloroethanol liquid was contained in a vertical stainless steel (SS) bottle (L = 30 cm, ID = 2.54 cm). Provision was made for bubbling nitrogen (N_2) at a constant flow rate through the liquid, using a vertical tube (ID = 0.3 cm, L = 26 cm) coaxially fitted inside the bottle. The top end of the tube was connected to the gas line using a $^1/_4$-in. on−off valve with Swagelok fittings. The bottom end of the tube was closed. The longitudinal section of the tube (1 cm from the bottom) was circumferentially perforated with 0.5-mm-sized holes spaced apart at a distance of 1 mm from each other. The entire perforated section of the tube was submerged in the liquid. The level of the liquid in the bottle was maintained sufficiently high, to provide adequate residence time to N_2 bubbles for complete saturation with 2-chloroethanol. The tubular bubbler assembly was wrapped with an insulated heating tape (1000 W) to maintain the liquid at a constant temperature. Therefore, the vapor pressure and the concentration (mole fraction) of 2-chloroethanol in the carrier N_2 gas were set constant at predetermined values. The temperature of the bubbler was controlled with the aid of a PID temperature controller (Fuji Electric Co., Japan).

The N_2 laden with 2-chloroethanol vapors was passed at a flow rate of 0.2 slpm through the tubular adsorber. The geometrical configuration of the adsorber was similar to that of the shell−tube bubbler assembly described in the preceding paragraph. The adsorber consisted of a vertical SS tube (ID = 2.0 mm, outer diameter of OD = 4 mm, L = 4.5 cm) coaxially and vertically fitted in a SS shell (ID = 1.5 cm, L = 9.0 cm) with provisions made for the gas inlet and outlet. The surface of the tube was perforated with holes 0.5 mm in diameter, with a center-to-center distance of 1 mm. The bottom end of the tube was closed. ACF was wrapped over the perforated section of the tube. N_2 saturated with 2-chloroethanol flowed into the perforated tube, and then radially outward through the wrapped ACF into the shell, before exiting from the outlet port. The shell was wrapped with heating tape (1000 W). The temperature was controlled with the aid of a PID temperature controller (Fuji Electric Co., Japan).

The effluent gaseous stream from the adsorber was passed to the analytical section consisting of a gas chromatography (GC) system (Nucon Eng. Co., India) that was equipped with a flame ionization detector (FID) and a data station. A computer was connected to the data station to store the data and the corresponding chromatograph. All the gaseous streams from cylinders to the bubbler and GC analyzer were passed through gas purifiers that contained silica gel to remove moisture. A Bronkhorst-made mass-flow controller (MFC) was used to regulate the flow rate of N_2.

3. SURFACE CHARACTERIZATION

3.1. Nitrogen Adsorption Isotherms and Data. The various adsorbents (ACF, Ni-ACF, Ni-ACF-pyridine, ACF-pyridine) prepared in this study were analyzed for the following properties: specific surface area, pore volume, and PSD by N_2-physisorption, using an Autosorb-1C instrument (Quantachrome, USA). In addition, chemisorption was also carried out to measure the active metal surface area. The multipoint Brunauer−Emmett−Teller (BET) surface area was measured from the nitrogen adsorption/desorption isotherm. The isotherm data were

Table 1. Specific Surface Area and Particle Size Distribution (PSD) of ACF, $NiNO_3$-ACF, NiO-ACF, Ni-ACF, and Functionalized ACF

sample	specific surface area (m^2/g) (N_2 BET)	total pore volume (cm^3/g)	PSD (%) micro	meso	macro
ACF	1256	0.721	87.17	7.5	5.33
0.4 M $NiNO_3$-ACF	1009	0.569	87.36	8.42	4.22
0.4 M NiO-ACF	1084	0.609	85.2	9.55	5.26
0.4 M Ni-ACF	1267	0.826	65.74	26.93	7.34
ACF-pyridine	1363	0.739	85.9	8.76	5.34
0.4 M Ni-ACF-pyridine	1027	0.563	87.22	8.37	4.41

experimentally determined using N_2 as an adsorbate gaseous molecule at 77 K.

The well-known BET equation, linearized as $1/[W(P_0/P) - 1]$ vs P/P_0, was applied to calculate the specific surface area of most of the porous solids. However, it may be noted that the BET adsorption isotherm is limited in the region of the P/P_0 range of 0.05−0.35, because the BET plot is usually linear in this range. Moreover, most of the micropores are filled in this range. Therefore, it has been suggested that, to calculate the multipoint BET surface area, the linear relationship of the BET equation should be maintained, which is usually in the range of $0.05 < P/P_0 < 0.35$. Attempts to determine the BET area by fitting the linearized form of the equation beyond $P/P_0 = 0.35$ to the isotherm data often result in unrealistic estimates.[27−29] Prior to the measurement, the samples were degassed at 200 °C for 8 h to remove any adsorbed water or entrapped gases in the ACF samples. The total pore volume was measured from the amount of vapor adsorbed at the relative pressure close to unity (0.9994).

Table 1 summarizes the results of the N_2 adsorption study. The data shown in rows 1 and 2 refer to ACF and $NiNO_3$-ACF, respectively. The incorporation of metals in ACF caused a decrease in both the surface area and the total pore volume, which is attributed to the dispersion of metal particles in the micropores of ACF. However, the area and pore volume largely recover, following H_2 reduction of the samples, as shown in row 4 of Table 1. On the other hand, the BET area and pore volume increase, although marginally, following the surface functionalization of ACF, as evident from the comparison of the data corresponding to sample numbers 1−5. The reason is attributed to the opening of pores by pyridine vapors during surface functionalization at 120 °C. In contrast, the surface area and pore volume considerably decrease following the functionalization of nickel-impregnated ACF (see rows 4 and 6 of Table 1). In this case, the effect of pore opening by pyridine is far outweighed by the formation of the tetrapyridine Ni complex salts, causing a net decrease in the BET area and pore volume. As discussed later in the paper, the adsorption capacity of the functionalized samples was determined to be significantly improved, in comparison to the original samples (ACF and Ni-ACF).

PSD was calculated from desorption isotherms by the Barrett−Joyner−Halenda (BJH) method for mesopores (2−40 nm), and the density functional theory (DFT) for micropores (<2 nm), assuming slit-type pores in ACF. As observed from Table 1, the micropore contents decreased following calcination and reduction of the impregnated samples, which enhances the mesopores, because these pores opened up due to heat treatment and reduction. This is shown in rows 2 and 4 of Table 1. The mesopore contents increased by a factor of ∼3, from 8.42% to 26.93%, because of calcinations followed by reduction. As also observed from the table, surface functionalization of ACF by pyridine resulted in a marginal increase of the mesopore contents. In contrast, functionalization of nickel-impregnated ACF (sample 4) by pyridine caused a substantial decrease in the mesopore contents, because of the formation of salts in the interior surfaces.

The main objective of the hydrogen (H_2) chemisorption analysis was to determine the active metal surface area. In a typical analysis, the samples were purged with hydrogen at 600 °C to clean the surface and convert uncatalyzed nickel oxide particles to their metallic state (nickel) before chemisorption was performed at 40 °C. The active metal surface area was determined to be 0.351 m^2/g-ACF. These data are later used in calculating the adsorptive loading of 2-chloroethanol in different metrics (g/g of ACF, g/m^2 of ACF, and g/m^2 of active metal surface area).

3.2. Scanning Electron Microscopy and Energy-Dispersive X-ray (EDX) Analysis. Field-emission scanning electron microscopy (FE-SEM) analysis (Supra 40 VP, Zeiss, Germany) was used to observe the surface morphology of ACF and Ni-ACF. The samples were coated with gold to improve their conductivity, so that good images could be obtained. In addition, EDX elemental spectra of a few spots on the samples were obtained, to determine the elemental compositions. Here, we present the representative images and spectra of the samples.

Figures 3a−c are SEM images of the as-received ACF samples at different magnifications. As observed, the external surface of the as-received ACF samples is smooth (Figure 3b). The pores in ACF also can be observed (Figure 3c). The EDX spectrum shown in Figure 3c suggests that no foreign metals are present as an impurity in the sample. Figures 4a−c are the SEM images of the ACF samples impregnated with metal (nickel) at different concentrations. It is evident that the surface of ACF becomes rougher than that of the as-received ACF following metal impregnation. The surface morphology of the nickel-impregnated ACF also exhibits grooves, which indicates that the surface is etched because of the incorporation of metals by impregnation. A salient observation is the increasing coverage of the ACF surface with increasing nickel concentration in the impregnating solvent. At a nickel concentration of 0.8 M, the external surface of ACF is, in fact, completely covered by nickel particles, thereby blocking the entrance to the pores of ACF. We revisit this aspect in the following section.

3.3. X-ray Diffraction Analysis. Powder X-ray diffraction (XRD) analysis was undertaken to determine the structural parameters of the prepared Ni-ACF samples, using a Seifert X-ray generator (ISO Debyeflex 2002, Germany) for the Cu Kα radiation. The finely powdered sample of ACF/Ni-ACF was placed on a cleaned glass plate as a thin layer for the analysis. The samples were analyzed over a 2θ range of 10°−80° at a step size of 0.5°.

The XRD patterns of ACF and Ni-ACF are shown in Figure 5. The broad diffraction peaks observed at 25° 2θ in all samples are related to the d_{002} plane, indicating that ACF has a cokelike character with a disordered carbonaceous interlayer.[30] However, the depth of the peaks decreases as the nickel concentrations increases, which reflects a change in the carbon structure from disordered (amorphous) carbon to ordered (crystalline) carbon. No presence of nickel particles is observed in the as-received

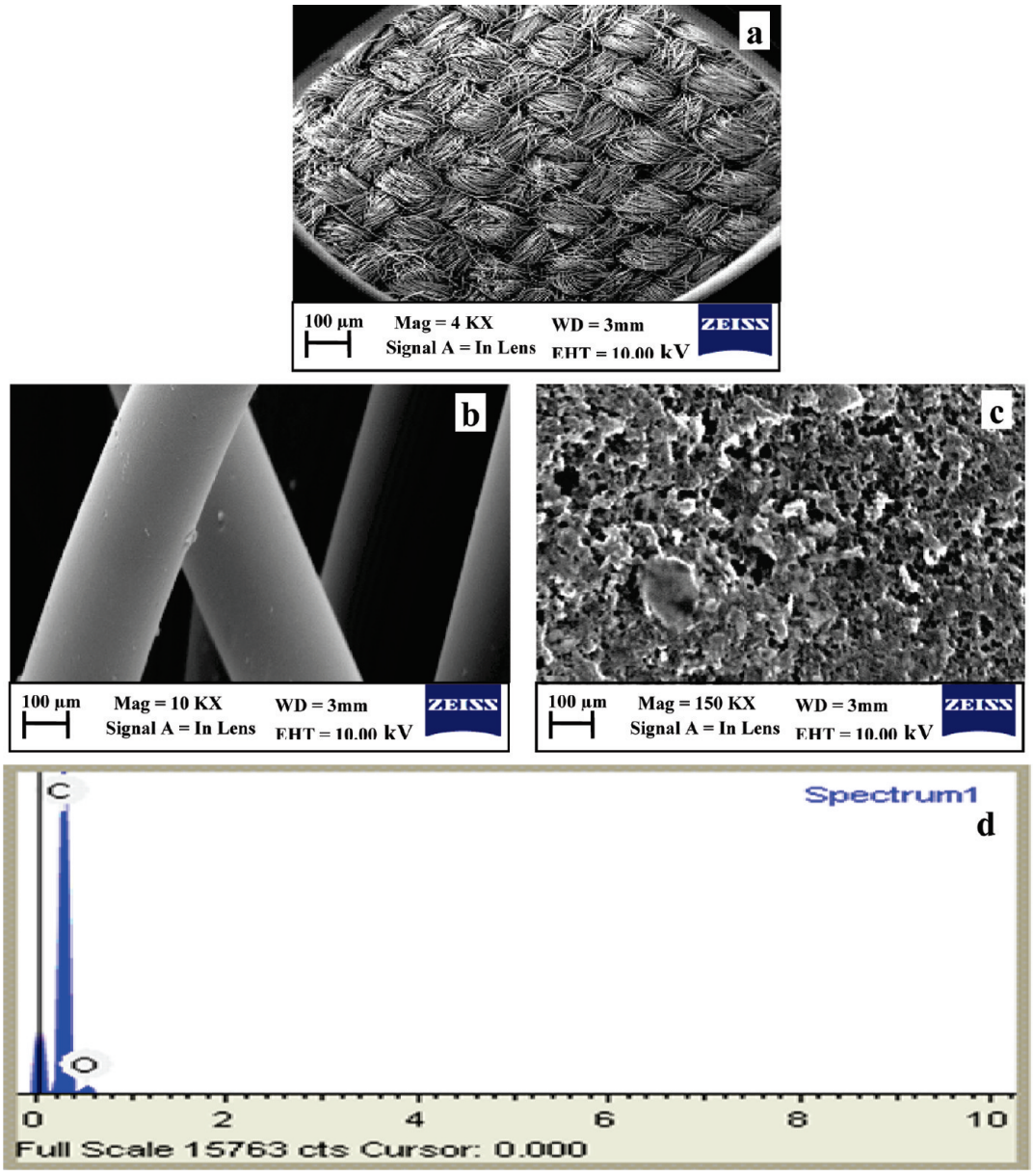

Figure 3. (a−c) Scanning electron microscopy (SEM) images of ACF at different magnfications. (d) Energy-dispersive X-ray (EDX) spectra of ACF.

ACF sample from the XRD analysis (see Figure 5a). However, the diffraction peaks observed at ∼44° 2θ and ∼51° 2θ are respectively assigned to (111) and (200) planes of nickel in its pure metallic state on the surface of Ni-ACF. At relatively lower concentrations, nickel is dispersed in ACF without the formation of large particles. However, at concentrations of 0.4 M or larger, the formation of large particles occurs. From Figure 5, it is also clear that the larger the metal concentration, the sharper the peak at ∼44° 2θ, which also indicates the formation of large crystals. Calculation of crystal size, using Scherrer's formula, yields an increase in the crystal (particle) size of nickel, from 4.35 nm (which corresponds to the 0.1 M Ni-ACF sample) to 74.16 nm (which corresponds to the 0.8 M Ni-ACF sample).

3.4. Fourier Transform Infrared (FT-IR) Spectroscopy. The FT-IR spectra of ACF and surface-functionalized ACF were acquired using a Tensor 27 apparatus (Bruker, Germany) in the attenuated total reflectance (ATR) mode, using crystalline germanium. Data acquisition was performed automatically using an interfaced computer and a standard software package. The samples were dried at 100 °C under vacuum prior to obtaining the spectra. The sample chamber was continuously purged with nitrogen during the measurement, to minimize the effect of atmospheric CO_2 and moisture. The background spectrum was obtained prior to the sample scanning. A total of 100 scans were taken for each sample. The resolution was set to 4 cm^{-1}, and atmospheric compensation was done to remove the atmospheric interference in the sample chamber.

Figure 6 describes the typical FT-IR spectra obtained for the raw and functionalized ACF. Differences in the surface functional groups of the two samples are observed. The peak at ∼3700 cm^{-1} corresponds to the N−H stretching of secondary amines with aromatic rings. The peaks in the region between ∼1650−1580 cm^{-1} corresponds to N−H bending from primary amines. The band at 1641 cm^{-1} refers to C═O bonds. The shifting of the carbonyl peak (from ∼1550 cm^{-1} to 1590 cm^{-1}) indicates the formation of carboxylate anion, which is attributed

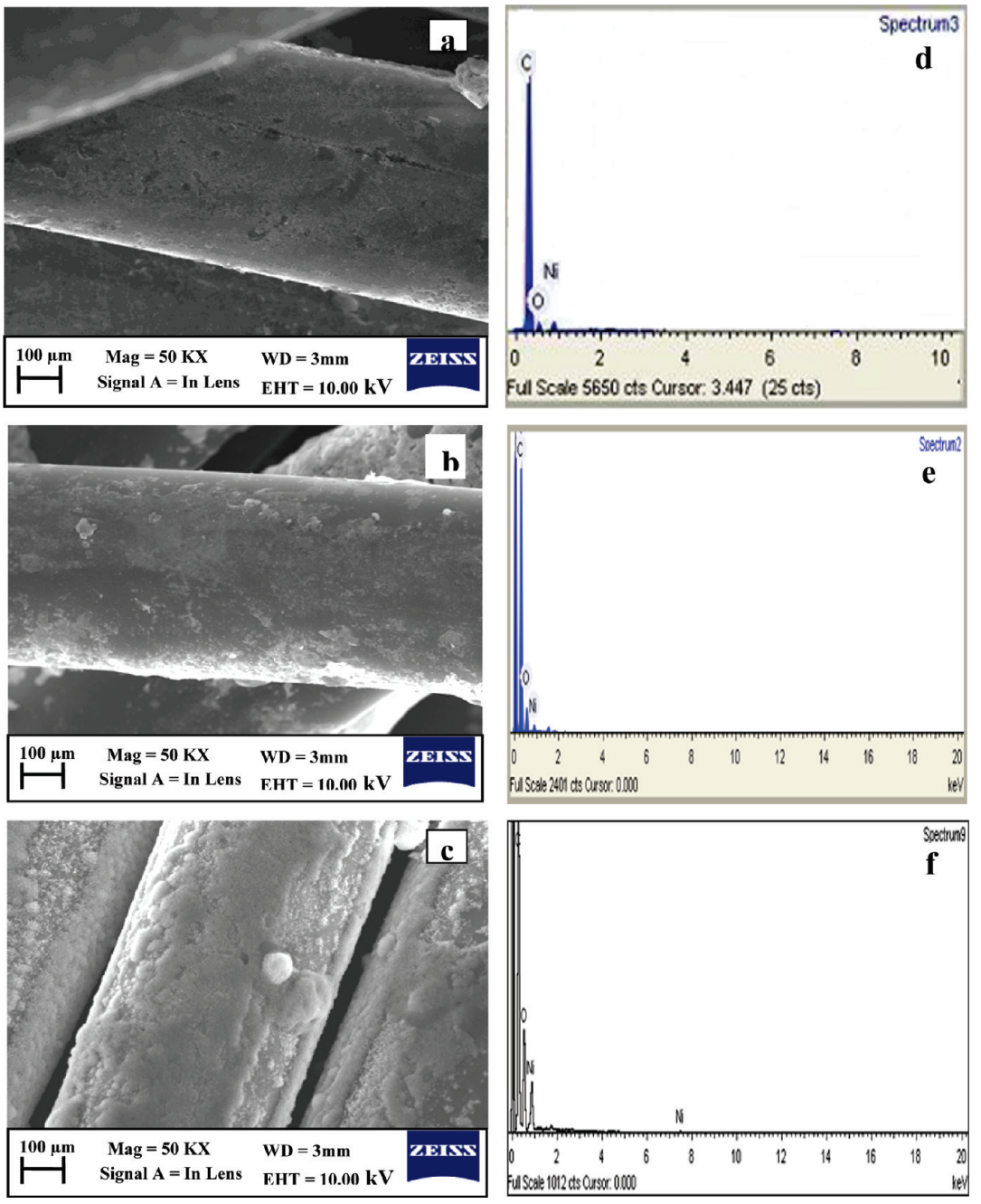

Figure 4. SEM images of ACF impregnated with nickel nitrate at different concentrations: (a) 0.1 M, (b) 0.4 M, and (c) 0.8 M. EDX spectra of ACF impregnated with nickel nitrate at different concentrations: (d) 0.1 M, (e) 0.4 M, and (f) 0.8 M.

to the deprotonation of carboxylic acid functionality. We revisit this aspect later in this paper, in the section on the proposed mechanism of adsorption for 2-chloroethanol on ACF and Ni-ACF.

3.5. Elemental Analysis (EA). Carbon (C), hydrogen (H), nitrogen (N), and oxygen (O) elemental analysis (EA) of the various samples was carried out with the aid of the elemental analyzer (Model CE-440 EL, Exeter Analytical, Inc., USA). The C, H, N, and O contents (expressed as a percentage) were determined for the various samples.

Table 2 describes the elemental compositions of ACF, $NiNO_3$-ACF, NiO-ACF, Ni-ACF, and pyridine-functionalized ACF. As observed, the amount (percentage by weight) of oxygen increased (by a factor of ~2) in the nickel-impregnated samples, compared to that in ACF, because of the incorporation of $NiNO_3$. However, the oxygen contents decreased following calcinations and reduction, because of the conversion of nitrates into oxides and reduction of oxides by H_2. As also observed, the amount of nitrogen, expressed as a percentage, expectedly increased following impregnation and decreased after calcinations. On the other hand, the amount of nitrogen and hydrogen increased in the functionalized samples, because of the deprotonation of acidic functionality, as shown in Table 2. The amounts of hydrogen and nitrogen increased to 1.92% and 3.53% in ACF-pyridine, and 2.17% and 4.13% in Ni-ACF-pyridine, respectively, from 1.02% and 0.27% in ACF. These increases are due to the introduction of N-functional groups during

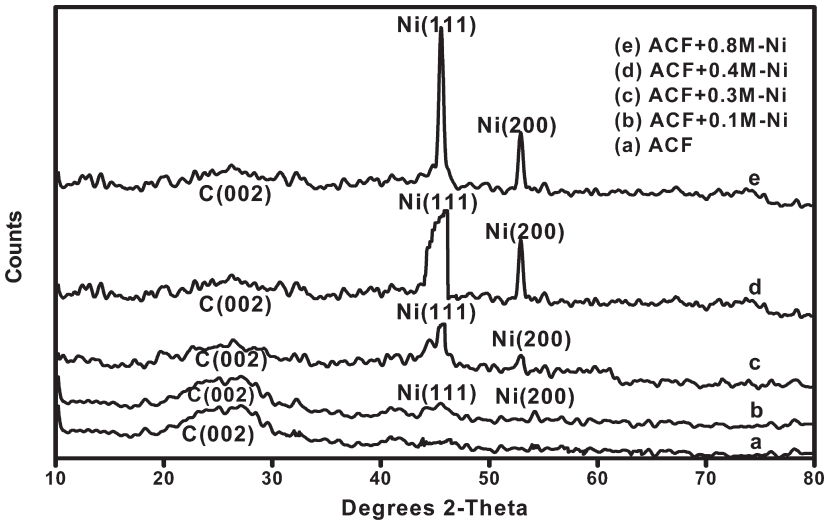

Figure 5. X-ray diffraction (XRD) spectra of ACF and the Ni-ACF samples.

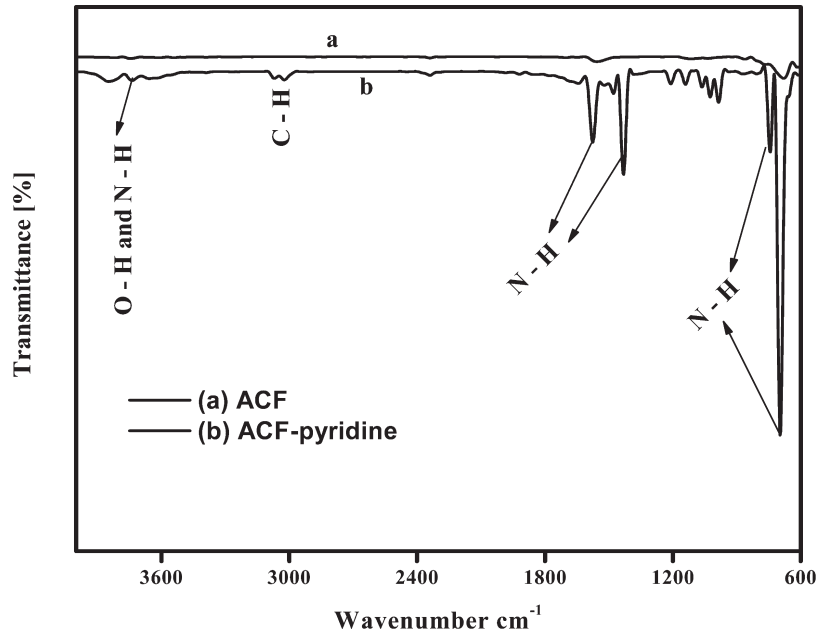

Figure 6. FT-IR (ATR) spectrum of ACF and functionalized ACF.

Table 2. Elemental Analysis Data of ACF, NiO-ACF, Ni-ACF, and Functionalized ACF

sample	Composition (%)				O/C ratio
	C	H	N	O	
ACF	89.16	1.02	0.27	9.05	1.02
0.4 M $NiNO_3$-ACF	76.50	2.95	2.77	17.29	0.98
0.4 M NiO-ACF	80.42	1.39	1.21	16.18	0.46
0.4 M Ni-ACF	83.90	1.59	1.05	13.44	0.16
ACF-pyridine	86.91	1.92	3.53	6.64	0.08
0.4 M Ni-ACF-pyridine	88.22	2.17	4.13	4.71	0.07

Table 3. Adsorptive Loading of 2-Chloroethanol on ACF, NiO-ACF, Ni-ACF, and Functionalized ACF

sample	loading (g/g of ACF)	loading (g/m^2 of ACF)	loading (g/m^2 of Ni)
ACF	0.316	0.00025	
0.4 M NiO-ACF	0.355	0.00032	1.01
0.4 M Ni-ACF	0.422	0.00033	1.201
ACF-pyridine	0.492	0.00036	
0.4 M Ni-ACF-pyridine	0.61	0.00059	1.737

functionalization. The important parameter that reflects changes in the elemental compositions at different intermediate processing steps is the O/C ratio, which was observed to decrease from 1.02 in ACF to 0.16 in Ni-ACF to 0.07 in Ni-ACF-pyridine samples.

As shown in Table 2, the O/C ratio is smaller in the functionalized ACF than the parent ACF. The data indicate the removal of

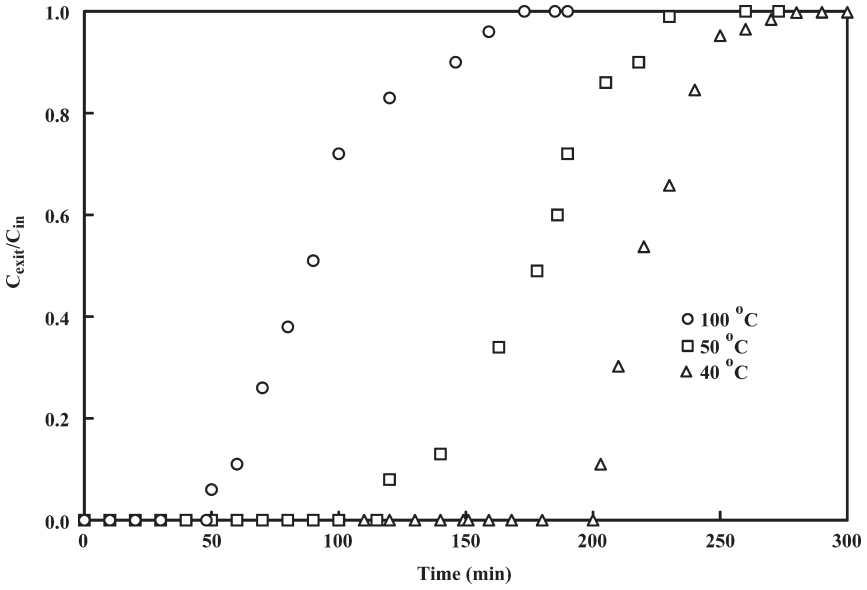

Figure 7. Adsorption of 2-chloroethanol under flow conditions for varying bed temperatures (amount of 0.4 M Ni-pyridine = 2 g, Q_{N_2} = 0.2 slpm, C_{in} = 7600 ppm).

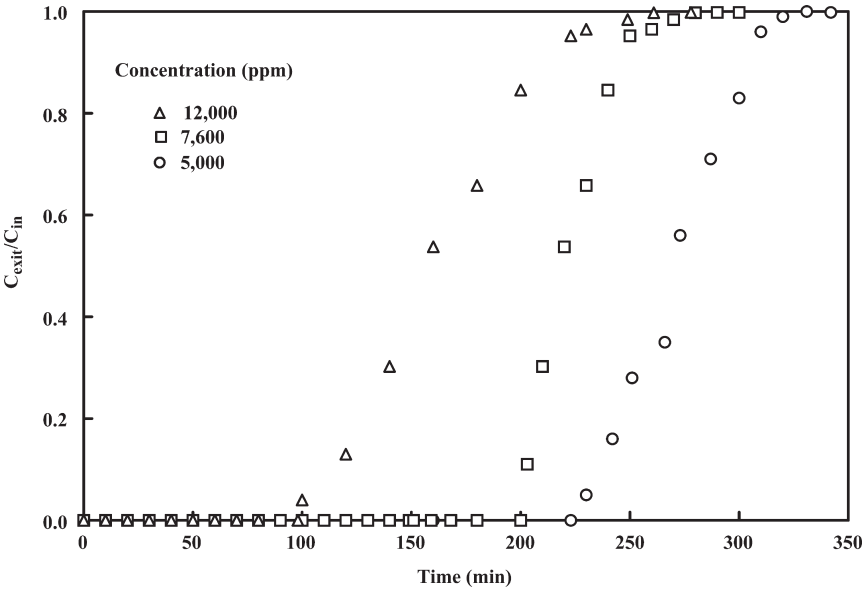

Figure 8. Adsorption of 2-chloroethanol under flow conditions for varying 2-chloroethanol concentrations (amount of 0.4 M Ni-pyridine = 2 g, Q_{N_2} = 0.2 slpm, T_{bed} = 313 K).

oxygen-containing groups by surface functionalization, which renders the surface basic. The adsorbate molecule, 2-chloroethanol, is strongly acidic. Therefore, it follows that the basic surface created by functionalization results in enhanced adsorption, because of the strong affinity of 2-chloroethanol molecules toward the basic sites of the surface, as corroborated from the comparative breakthrough data for the functionalized and nonfunctionalized ACF discussed later in the paper. As also evident from the data presented in Table 3, the adsorption capacity is larger for the functionalized ACF samples than ACF, because of the relatively smaller O/C ratio, which reflects the relatively larger basicity of the functionalized surface.

4. BREAKTHROUGH STUDY OF 2-CHLOROETHANOL

Figures 7−10 describe the results of the adsorption tests carried out for 2-chloroethanol on ACF, Ni-ACF, and the functionalized ACF under flow conditions. The results are the breakthrough data obtained under different experimental conditions. In a typical experiment, the test sample was wrapped on the tubular perforated adsorber and 2-chloroethanol-laden nitrogen gas at a predetermined concentration was continuously fed at a constant flow rate to the adsorber. For the purpose of comparing the performance of the adsorbent under different conditions, breakthrough time was taken as the time when the effluent concentration increases to ∼1% of the inlet concentration. Similarly, the saturation time was taken as the time when the effluent concentration level reaches ∼99% of that at the inlet.

Figures 7 and 8 describe the typical breakthrough curves obtained under different temperatures and concentrations, respectively. The adsorption bed remains fully effective until a small concentration of the analyte is observed at the exit of the

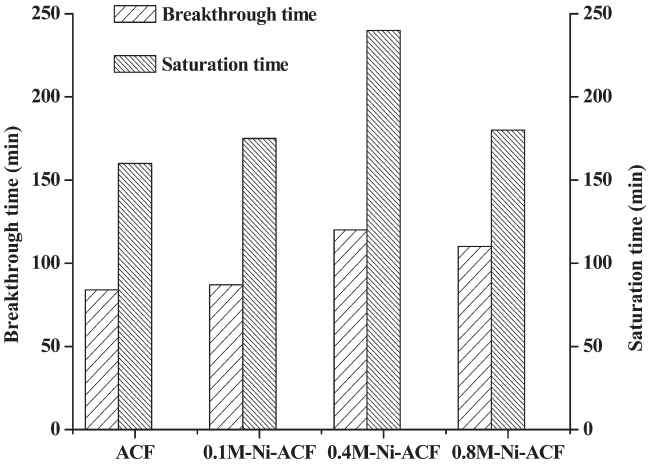

Figure 9. Comparison of breakthrough and saturation times for different nickel nitrate concentrations of ACF, 0.1 M Ni-ACF, 0.4 M Ni-ACF, and 0.8 M Ni-ACF (amount of ACF = 1.5 g, Q_{N_2} = 0.2 slpm, T_{bed} = 313 K, C_{in} = 7600 ppm).

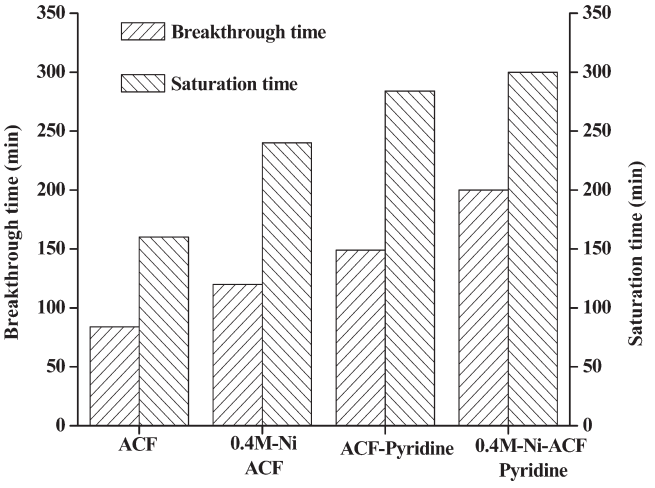

Figure 10. Comparison of breakthrough and saturation times for different adsorbents of ACF, 0.4 M Ni-ACF, ACF-pyridine, and 0.4 M Ni-ACF-pyridine (amount of ACF = 2 g, Q_{N_2} = 0.2 slpm, T_{bed} = 313 K, C_{in} = 7600 ppm).

tube. After the breakthrough, the exit concentration gradually increases until it asymptotically reaches the inlet gas concentration. The bed is now fully saturated with no remaining capacity for further adsorption. The important observation to make from Figure 7 is the adverse effect of temperature on adsorption. As the temperature is increased from 40 °C to 100 °C, the breakthrough and saturation times decrease, which suggests that the (adsorptive) removal of 2-chloroethanol becomes less effective at relatively larger temperatures. This is also observed from the breakthrough curves, where the equilibrium solute loading (proportional to the area above the curve) decreases as the temperature increases. It is also evident from Figure 8 that breakthrough time decreases as the inlet concentration increases, as expected. At large influent concentrations, the effluent concentration of 2-chloroethanol is observed to increase rapidly with an early saturation of the bed.

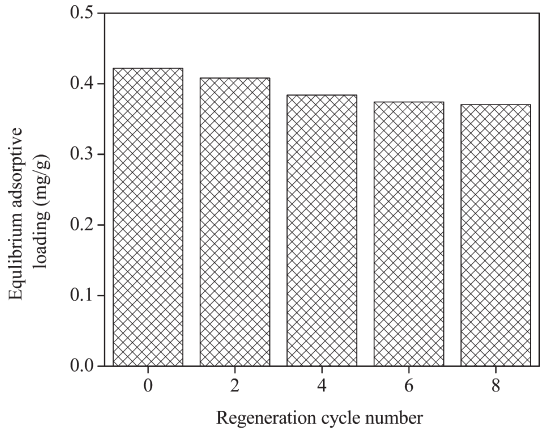

Figure 11. Adsorption capacity of 0.4 M Ni-ACF after successive adsorption/regeneration cycles.

In addition to ascertaining the effects of temperature and concentration on adsorption, the influence of metal (nickel) loading of ACF and the adsorptive characteristics of the adsorbents at different stages of preparation were also investigated under flow conditions. Here, we present the comparative data for breakthrough and adsorption times in Figures 9 and 10, obtained from the respective breakthrough curves for these two cases.

As observed from Figure 9, breakthrough and saturation times increased as the nickel concentrations increased from 0.1 M to 0.4 M in the impregnating solvent. The reason is attributed to the fact that the number of available active metal sites increases as the metal concentrations increase, resulting in enhanced adsorption of the solutes and, consequently, large equilibrium loadings of adsorbate molecules. Therefore, the breakthrough and saturation times also increase.

However, the extent of adsorption decreased with early breakthrough and saturation of the bed, corresponding to 0.8 M Ni-ACF, as indicated in the earlier sections on XRD data in this paper. The results are consistent with the fact that, beyond a certain concentration level (0.4 M) in the impregnating solvent, the formation of metal crystallites of relatively larger size occurred, resulting in the almost-complete coverage of the external surface of ACF and causing the blockage of the pores and, therefore, the adverse performance of the adsorbent.

Under the experimental conditions of this study, the surface started to be covered with large nickel particles because of agglomeration at nickel concentrations of >0.4 M in the impregnating solvent. At a nickel concentration of 0.8 M, the external surface was almost completely blocked, as shown in Figure 3c. To be on the safe side, we set the nickel concentration of the impregnating solvent to 0.4 M for uniformly impregnating the ACF with nickel particles without agglomeration.

Figure 10 compares the breakthrough and saturation times for different adsorbents (ACF, 0.4 M Ni-ACF, ACF-pyridine, and 0.4 M Ni-ACF-pyridine). The two times are observed to be larger for Ni-ACF than the parent material, ACF, because of the incorporation of nickel in the adsorbent. The functionalization of ACF and Ni-ACF by pyridine also results in increases in the breakthrough and adsorption times, because of the incorporation of the basic functional groups, indicative of the superior performance of the pyridine-functionalized 0.4 M Ni-ACF, in comparison to the parent substrate material (ACF) or the intermediate material (Ni-ACF). The results clearly suggest that both metal impregnation and the creation of the basic surface result in

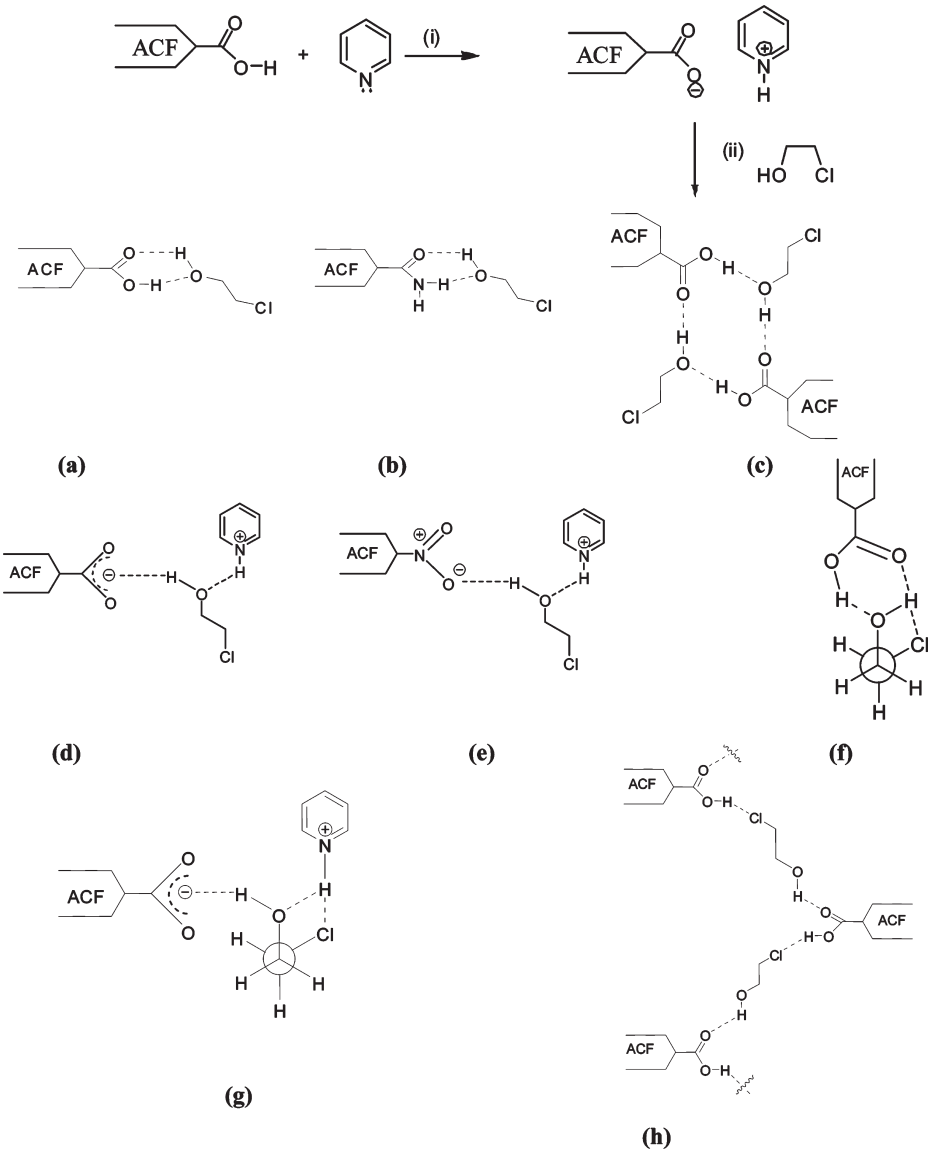

Figure 12. Proposed mechanism for the functionalization of ACF and adsorption of 2-chloroethanol on the surface-functionalized ACF. Step (i) depicts deprotonation of the carboxylic acid functionality of ACF by pyridine, while step (ii) shopws different hydrogen-bonded motifs (a−h), which may be responsible for the binding of 2-chloroethanol.

enhanced adsorptive capacity of the prepared adsorbent for the organic solute.

Calculation was done to estimate the effective diffusion coefficient of 2-chloroethanol in the metal-impregnated ACF. The calculation considered combined molecular and pore diffusion effects. The pore diffusion coefficient is dependent on the PSD of the material (metal-impregnated ACF). The PSD data are presented in Table 1. Based on the average pore size of the micropores in ACF, the effective pore diffusivity was calculated to be 3.084×10^{-8} m^2/s, which is of the same order of magnitude as that reported in the literature for gaseous hydrocarbon molecules in ACF.[31,32] The detailed calculation is presented in the Appendix.

The solute loading (w/w) on the adsorbents may be determined from the total uptake of the solute, by calculating the integral along the breakthrough curve between the two time limits: the incipience of adsorption test (step change in the inlet concentration) and the instance when the bed is saturated. Mathematically, the uptake of the solute (expressed in milligrams) is determined as follows:

$$\text{uptake (mg)} = Q\left(C_{in}T - \int_0^T C_{exit}\, dt\right)$$

where T is the total time of adsorption until the bed is saturated with the solute in the influent stream, C_{in} the inlet concentration of the adsorbate, and C_{exit} the exit concentration of the adsorbate. Table 3 summarizes the experimentally obtained values for the adsorptive loading of 2-chloroethanol in different metrics. As observed, the loading of 2-chloroethanol on 0.4 M Ni-ACF-pyridine is the largest at ~0.6 g/g, which is approximately double that of the parent substrate, ACF, alone. With the BET surface area and active metal surface area of 0.4 M Ni-ACF-pyridine measured at 1027 m^2/g and 0.351 m^2/g, respectively, loading of 2-chloroethanol also may be expressed in other metrics, for example, ~0.00059 g/m^2, based on the BET surface area of ACF,

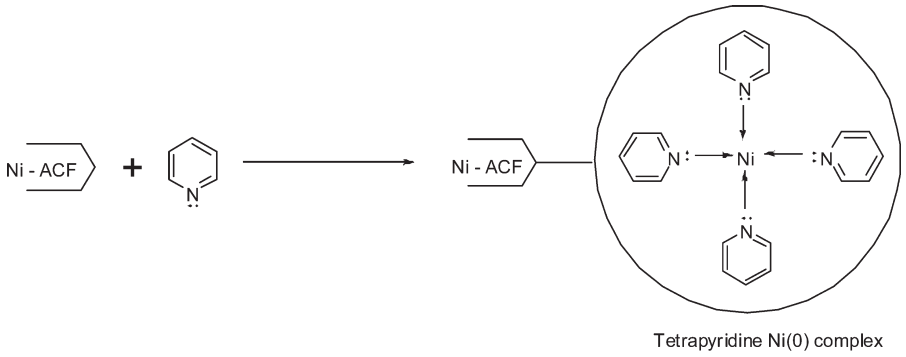

Figure 13. Proposed mechanism for the functionalization of ACF and adsorption of 2-chloroethanol on the surface functionalized ACF. Tetrapyridine Ni(0) complex is formed on functionalization of Ni-ACF by pyridine.

and 1.74 g/m^2, based on the active metal surface area. These data on the functionalized ACF may be compared to the corresponding loading on the nonfunctionalized metal-impregnated ACF: 0.42 g/g of ACF, 0.00033 g/m^2 based on the BET surface area of ACF, and 1.2 g/m^2 of active metal surface area. Thus, there is a significant improvement of the adsorption capacity of the prepared adsorbent via the surface functionalization presented herein.

We have also compared the adsorption capacity of the prepared adsorbents in this study to the reported literature data for a few toxic organic compounds, because of nonavailability of the data for 2-chloroethanol. The as-received pitch-based ACF has been tested for the removal of dimethyl methylphosphonate (DMMP) and carbon tetrachloride (CCl_4), which are common simulants for chemical warfare agents.[33] From the experimental breakthrough curves, the equilibrium loadings of DMMP and CCl_4 on ACF at 25 °C were obtained as ∼0.59 g/g and ∼0.194 g/g of ACF, respectively. In the aforementioned study, the authors also prepared metals (Ag/Cu/Cr)-impregnated activated-carbon granules. However, the adsorption capacity of the prepared materials obtained was relatively lower, at ∼0.08 g/g and ∼0.01 g/g for DMMP and CCl_4, respectively.

Regeneration tests also were carried out on the spent Ni-ACF samples to ascertain their reusability following regeneration. The tests were carried out in situ, using hot air, under flow conditions. After saturation of the adsorbents in the adsorption step, the inlet gas line to the tubular adsorber was switched to that of air at a flow rate of 100 sccm. The temperature of the adsorber was held at 200 °C. The concentration of 2-choloroethanol vapors at the exit of the adsorber was measured until no vapor was detected in the effluent air. Under the present regeneration conditions, the regeneration time was observed to vary between 30 min to 45 min, depending on the samples that were pre-equilibrated at different concentration levels (5000−12000 ppm) of 2-choloroethanol vapors during the adsorption step. The regenerated adsorbent was reused in the subsequent adsorption test and the equilibrium loading was recalculated from the corresponding breakthrough curve. Such adsorption−desorption (regeneration) cycle was repeated several times.

The equilibrium adsorptive loading data for fresh and regenerated samples are presented in Figure 11. The results are shown for the samples pre-equilibrated at 5000 ppm. As observed from the figure, the adsorption capacity of the sample decreased by ∼15% after 2-cycles. The subsequent cycles yielded in marginal reduction of the capacity, suggesting effectiveness of regeneration using hot air, and reusability of the prepared adsorbents in the subsequent removal of 2-chloroethanol in the adsorption step. Visual examination of the samples did not show any perceptible adverse change in the surface of ACF or damage to the fabrics. We plan to address the regeneration, in a separate study.

5. PROPOSED MECHANISM OF SURFACE FUNCTIONALIZATION AND ADSORPTION OF 2-CHLOROETHANOL

Figure 12 describes a possible mechanism of the surface functionalization of ACF by pyridine and subsequent adsorption of 2-chloroethanol on the surface-functionalized ACF. As shown in the figure, deprotonation of carboxylic acid functionality occurs during reflux of pyridine vapors on ACF, resulting in the formation of pyridinium carboxylate. In this step, the acidic functionalities of the surface decrease, whereas the basic groups remain intact. The overall effect is to increase the basicity of the ACF surfaces. The resultant salts formed by pyridine with the carboxylic groups of ACF evidently exhibit enhanced binding propensity for 2-chloroethanol. The interactions shown in Figures 12a−h could presumably be responsible for the observed increase in the adsorption of 2-chloroethanol by pyridine-treated ACF. Note that there is a wealth of literature that is constantly expanding on heterosynthons,[34−36] which represents interaction motifs between two or more different functional groups.

Figure 13 describes a mechanism for the functionalization of nickel-impregnated ACF (Ni-ACF) and the adsorption of 2-chloroethanol on the functionalized Ni-ACF. As shown in the figure, functionalization results in the coordination of Ni with four molecules of pyridine, forming a neutral complex molecule, tetra pyridine Ni(0). The effect is an increase in the adsorption capacity of Ni-ACF, because of the chemical interaction between nickel and 2-chloroethanol. Here, it is important to note that the steps outlined in Figure 12 for the adsorption of 2-chloroethanol on ACF without metal impregnation are also involved in adsorption on the sites unoccupied by Ni on Ni-ACF.

6. CONCLUSIONS

Activated carbon fiber (ACF) materials that have been impregnated with nickel and functionalized with pyridine were found to have a significant adsorption capacity for 2-chloroethanol. Temperatures well above 40 °C adversely affected the adsorption of 2-chloroethanol. The superior adsorption of Ni-ACF was ascribed to the large concentration of active sites, for

which nickel plays an important role during adsorption. However, at nickel concentrations in excess of 0.4 M, the formation of metal crystallites occurred, causing the blockage of pores of ACF, which, in turn, adversely affected the adsorptive performance of the prepared adsorbents. The surface functionalization by pyridine was shown to yield a basic surface, which significantly enhanced the adsorption capacity. The repeat adsorption/desorption tests showed that at least 85% of the initial adsorption capacity of Ni-ACF for 2-chloroethanol may be recovered by regeneration using hot air at 200 °C. The study assumes significance from the perspective of developing suitable metals-impregnated and surface-functionalized ACF-based adsorbents for the control of toxic organic pollutants.

APPENDIX

The effective diffusion coefficient (D_{eff}) of a species in the porous adsorbent material is determined as follows:[37]

$$D_{eff} = \alpha D/\tau$$

where α is the intrafiber void fraction, τ the tortuosity factor, and D the combined diffusivity coefficient. D is calculated from the molecular diffusivity (D_m) and the Knudsen diffusivity (D_k) as follows:

$$D = \frac{1}{(1/D_m) + (1/D_k)}$$

D_k is calculated from the following empirical equation:

$$D_k\ (m^2/s) = 97 r_{pore} \left(\frac{T}{M}\right)^{1/2}$$

where r_{pore} is the pore radius (expressed in meters), M the molecular weight (expressed in units of g/mol), and T the temperature (in Kelvin).

The parameter D_m (m^2/s) for a binary gas mixture is evaluated using the Chapman−Enskog equation:

$$D_m = \frac{0.0018583(10^{-4})T^{3/2}\left[(1/M_A) + (1/M_B)\right]^{1/2}}{P\sigma_{AB}{}^2\Omega_{AB}}$$

where M_A and M_B are the molecular weights of nitrogen and 2-chloroethanol, respectively. Ω is the collision integral, which is a function of k_bT/ε_{AB} (where k_b is the Boltzmann's constant). The terms σ_{AB} (expressed in Angstroms) and ε_{AB} are constants in the Lennard-Jones potential-energy function for the pair of molecules A and B.

Substituting the average pore size of micropores, $r_{pore} = 1.06 \times 10^{-9}$ m, $\alpha = 0.63$, $\tau = 4$ into the above equations, D_m and D_k were calculated to be 5.75296×10^{-6} m^2/s and 2.02721×10^{-7} m^2/s, respectively. D_{eff} was calculated as 3.084×10^{-08} m^2/s.

AUTHOR INFORMATION

Corresponding Author

*Tel.: +91-512-2596124. Fax: +91-512-2590104. E-mail: nishith@iitk.ac.in.

ACKNOWLEDGMENT

The authors acknowledge the support from DRDO, New Delhi in the form of a research grant, and DST unit on Nanosciences, IIT Kanpur. The authors also acknowledge the supply of ACF from Kynol, Inc., Japan.

REFERENCES

(1) Phipps, G. L.; Holecombe, G. W. A method for aquatic multiple species toxicant testing: cute toxicity of 10 chemicals to 5 vertebrates and 2 invertebrates. *Environ. Pollut. A* **1985**, *38*, 141–157.

(2) Pace, G.; Berton, A.; Calligaro, L.; Mantovani, A.; Uguagliati, P. Elucidation of the degradation mechanism of 2-chloroethanol by hydrogen peroxide under ultraviolet irradiation. *J. Chromatogr. A* **1995**, *706*, 345–351.

(3) Dijk, J. A.; Stams, A. J. M.; Schraa, G.; Ballerstedt, H.; de Bont, J. A. M.; Gerritse, J. Anaerobic oxidation of 2-chloroethanol under denitrifying conditions by *Pseudomonas Stutzeri* strain JJ. *Appl. Microbiol. Biotechnol.* **2003**, *63*, 68–74.

(4) MacCann, J.; Simmon, V.; Streitwieser, D.; Ames, B. N. Mutagenicity of chloroacetaldehyde, a possible metabolic product of 1,2-dichloroethane (ethylene dichloride), chloroethanol (ethylene chlorohydrin), vinyl chloride, and cyclophosphamide. *Proc. Natl. Acad. Sci. USA* **1975**, *72* (8), 3190–3193.

(5) Xu, L.; Lin, G.; Wang, X.; Lin, R. Densities and volumetric properties of 2-chloroethanol with *N*,*N*-dimethylformamide and water at different temperatures. *J. Mol. Liq.* **2006**, *123*, 130–133.

(6) Gaur, V.; Asthana, R.; Verma, N. Removal of SO_2 by activated carbon fibers in presence of O_2 and H_2O. *Carbon* **2006**, *44*, 46–60.

(7) Gaur, V.; Sharma, A.; Verma, N. Preparation and characterization of ACF for the adsorption of BTX and SO_2. *Chem. Eng. Process.* **2006**, *45*, 1–13.

(8) Singh, B.; Madhusudhan, S.; Dubey, V.; Nath, R.; Rao, N. B. S. N. Active carbon for removal of toxic chemicals from contaminated water. *Carbon* **1996**, *34* (3), 327–330.

(9) Reucroft, P. J.; Chiou, C. T. Adsorption of cyanogen chloride and hydrogen cyanide by activated and impregnated carbons. *Carbon* **1977**, *15*, 285–290.

(10) Barnir, Z.; Aharoni, C. Adsorption of cyanogen chloride on impregnated active carbon. *Carbon* **1975**, *13*, 363–366.

(11) Freeman, G. B.; Reucroft, P. J. Adsorption of HCN and H_2O vapor mixtures by activated and impregnated carbons. *Carbon* **1979**, *17*, 313–316.

(12) Prasad, G. K.; Singh, B.; Suryanarayana, M. V. S.; Batra, B. S. Kinetic degradation of sulphur mustard on impregnated carbons. *J. Hazard. Mater. B* **2005**, *121*, 159–165.

(13) Jianying, W.; Fengyun, Z.; Yongqi, H.; Ruihong, Z.; Runjing, L. Modification of activated carbon fiber by loading metals and their performance on SO_2 removal. *Chin. J. Chem Eng.* **2006**, *14* (4), 478–485.

(14) Hong, I.; Jiang, H.; Park, Y. D.; Kim, J. Y.; Ha, B. H. Metal dispersed activated carbon fibers and their application for removal of SO_x. *Chem. Phys. Lett.* **2002**, *366*, 572–577.

(15) Das, D.; Gaur, V.; Verma, N. Removal of volatile organic compound by activated carbon fiber. *Carbon* **2004**, *42*, 2949–2962.

(16) Singhal, R. M.; Sharma, A.; Verma, N. Micro-nano hierarchal web of activated carbon fibers for catalytic gas adsorption and reaction. *Ind. Eng. Chem. Res.* **2008**, *47*, 3700–3707.

(17) Dwivedi, P.; Gaur, V.; Sharma, A.; Verma, N. Comparative study of removal of volatile organic compounds by cryogenic condensation and adsorption by activated carbon fiber. *Sep. Purif. Technol.* **2004**, *39* (1−2), 23–37.

(18) Gupta, A. K.; Deva, D.; Sharma, A.; Verma, N. Adsorptive removal of fluoride by micro-nano hierarchal web of activated carbon fibers. *Ind. Eng. Chem. Res.* **2009**, *48* (21), 9697–9707.

(19) Kang, K. C.; Kima, S. S.; Choi, J. W.; Kwon, S. H. Sorption of Cu^{2+} and Cd^{2+} onto acid-and base-pretreated granular activated carbon and activated carbon fiber samples. *Ind. Eng. Chem. Res.* **2008**, *14*, 131–135.

(20) Han, Y.; Quan, X.; Chen, S.; Zhao, H.; Cui, C.; Zhao, C. Y. Electrochemically enhanced adsorption of aniline on activated carbon fibers. *Sep. Purif. Technol.* **2006**, *50*, 365–372.

(21) Cui, C.; Quan, X.; Chen, S.; Zhao, H. Adsorption and electrocatalytic dechlorination of pentachlorophenol on palladium-loaded activated carbon fibers. *Sep. Purif. Technol.* **2005**, *47*, 73–79.
(22) Rathore, R. S.; Srivastava, D. K.; Agarwal, A. K.; Verma, N. Development of surface functionalized activated carbon fiber for control of NO and particulate matter. *J. Hazard. Mater.* **2010**, *173*, 211–222.
(23) Hattori, Y.; Noguchi, N.; Okino, F.; Touhara, H.; Nakahigashi, Y.; Utsumi, S.; Hideki, T.; Hirofumi, K.; Katsumi, K. Defluorination-enhanced hydrogen adsorptivity of activated carbon fibers. *Carbon* **2007**, *45*, 1391–1395.
(24) Mangun, C. L.; Benak, K. R.; Economy, J.; Foster, K. L. Surface chemistry, pore sizes and adsorption properties of activated carbon fibers and precursors treated with ammonia. *Carbon* **2001**, *39*, 1809–1820.
(25) Raymundo-Pinero, E.; Cazorla-Amoros, D.; Linares-Solano, A. The role of different nitrogen functional groups on the removal of SO_2 from flue gases by N-doped activated carbon powders and fibres. *Carbon* **2003**, *41*, 1925–1932.
(26) Material Safety Data Sheet, Nickel(II) Nitrate Hexahydrate 99%, 2010. Available online at http://avogadro.chem.iastate.edu/MSDS/Ni%28NO3%292-6H2O.htm (accessed November 2010).
(27) Stoekli, F.; Centeno, T. A. On the determination of surface areas in activated carbons. *Carbon* **2005**, *43* (6), 1184–1190.
(28) Cuerda-Correa, E. M.; Macias-Garcia, A.; Diez, M. A. D.; Ortiz, A. L. Textural and morphological study of activated carbon fibers prepared from kenaf. *Microporous Mesoporous Mater.* **2008**, *111*, 523–529.
(29) Condon, J. B. *Surface Area and Porosity Determinations by Physisorption Measurements and Theory*, 1st ed.; Elsevier B.V.: Oxford, U.K., 2006.
(30) Park, S. J.; Jang, Y. S. Preparation and characterization of activated carbon fibers supported with silver metal for antibacterial behaviour. *J. Colloid Interface Sci.* **2003**, *261*, 238–243.
(31) Adapa, S.; Gaur, V.; Verma, N. Catalytic oxidation of NO by activated carbon fiber (ACF). *Chem. Eng. J.* **2006**, *116*, 25–37.
(32) Cheng, T.; Jiang, Y.; Zhang, Y.; Liu, S. Prediction of breakthrough curves for adsorption on activated carbon fibers in a fixed bed. *Carbon* **2004**, *42* (15), 3081–3085.
(33) Ryu, S. K.; Choi, S. R. Activated carbon fibers for the removal of chemical warfare simulants. *J. Ceram. Soc. Jpn.* **2004**, *112* (5), 1539–1542.
(34) Desiraju, G. R. Supramolecular synthons in crystal engineering—A new organic synthesis. *Angew. Chem., Int. Ed. Engl.* **1995**, *34*, 2311–2327.
(35) Lehn, J. M. *Supramolecular Chemistry*; VCH: Weinheim, Germany, 1995.
(36) Desiraju, G. R. *Comprehensive supramolecular Chemistry*, 6th ed.; Pergamon Press: Oxford, U.K., 1996.
(37) Cussler, E. L. *Diffusion Mass Transfer in Fluid Systems*, 2nd ed.; Cambridge University Press: Oxford, U.K., 1998.